# 183. Structure and Dynamics of Intramolecular Hydrogen Bonds in Radicals: Substituent, Steric and Solvent Effects

by **Klaus Loth** and **Federico Graf**

Laboratory for Physical Chemistry, Swiss Federal Institute of Technology, CH-8092 Zürich, Switzerland

(28.I.81)

*Summary*

The temperature and solvent dependence of the ESR. spectra of a number of semiquinone- and semidione-type radicals have been investigated with the aim of obtaining structural and kinetic information about intramolecular hydrogen bonding. Systematic variation of the chemical structure of the radicals indicates that in many cases formation and/or exchange of intramolecular H-bonds is disturbed or even precluded by steric hindrance or concomitant dynamic processes, such as internal rotation and/or intermolecular proton exchange.

**1. Introduction.** – Hydrogen bonding association equilibria have been studied by NMR. spectroscopy for a large number of systems [1], but only in exceptional cases could dynamic information be retrieved from the spectra. For instance, with systems such as porphyrins [2][3] and 2,5-dihydroxy-*p*-benzoquinone [4] has it been possible to obtain information about the mechanism and the rate of intramolecular proton transfer processes from NMR. solution studies. This is often due to the fact that such processes take place at a rate which is too high to be resolved by NMR. Also because of the moderate sensitivity of this method, rather concentrated solutions have to be used, which in turn complicates the study of intramolecular phenomena owing to the presence of concomitant intermolecular processes [5]. ESR. spectroscopy does not have these disadvantages to the same degree because of the much larger dynamic range and of the higher sensitivity. In earlier papers, the intramolecular rotation of hydroxyl groups has been postulated from the interpretation of the line shape of the tetrahydroxynaphthalene cation by *Carrington et al.* [6] and of the *p*-hydroxyphenoxy radical by *Gough* [7]. The above process has been studied later in more detail, both experimentally [8][9] and theoretically [10], for the case of the hydroxymethyl radical. Another process related to H-bonding, the intramolecular proton transfer of the 2-hydroxyphenoxyl radical [11], has been thoroughly studied by the authors and independently by *Prokofiev et al.* [12].

More recently, it has been shown that, in connection with intramolecular H-bonding additional dynamic processes accessible to investigation by ESR. spectroscopy, such as the internal rotation around a C,C-bond [13], can take place. Furthermore, it also has become clear that even in the case of high dilution of a

0018-019X/81/6/1910-20$01.00/0 

molecular radical with hydroxyl groups and/or intramolecular hydrogen bridges, the interaction with the solvent can be an important or even determining factor for the ESR. line shape [14].

We show here that the chemical structure and the nature of the solvent largely determine whether intramolecular or intermolecular dynamic processes affect the ESR. line shape of a molecular radical subjected to H-bonding interaction. For some of the examples it will be shown that dynamic ESR. spectroscopy of high diluted solutions in non-polar solvents, supported by quantum chemical calculations, provides direct information about the structure and dynamics of H-bonds in radicals which cannot be obtained by other methods.

**2. Experimental part.** 2.1. *Materials, preparation of solutions and instrumentation.* The following substances were used for producing radicals: pyrocatechol (**I**-$H_2$), 4-methylpyrocatechol (**II**-$H_2$), 2-aminophenol (**III**-$H_3$), biacetyl (**5**) and benzil (**6**) *(Scheme 1).* All substances and solvents were commercially available and were used after purification by recrystallisation or destillation (*cf.* [11]). The preparation of the solutions and the instrumentation were basically the same as in [11].

Scheme 1. *Reactant molecules for the production of radicals which might exhibit intramolecular hydrogen bonds.* From pyrocatechol (**I**-$H_2$), 4-methylpyrocatechol (**II**-$H_2$) and 2-aminophenol (**III**-$H_3$) phenoxy type radicals were obtained by photooxidation. From glyoxal (**IV**), biacetyl (**V**) and benzil (**VI**) the radicals were produced by hydrogen abstraction from the solvent.

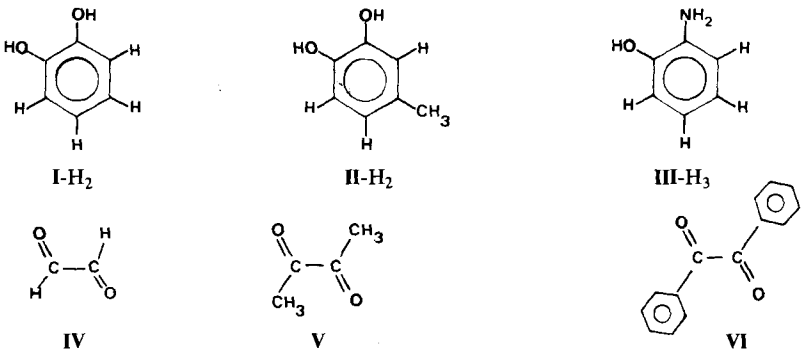


2.2. *Production of radicals.* The radicals were produced by photolyzing the oxygen-free solution directly in the microwave cavity. Depending on the type of radical, different methods were applied. Direct photooxidation *(equ. 1)* was used to produce the

$$\mathrm{ArOH} \xrightarrow{h\nu} \mathrm{ArO}\cdot + \mathrm{H}\cdot \qquad (1)$$

2-hydroxyphenoxyl (**I**-$H_2$), the 2-hydroxy-4-methylphenoxyl (**II**-$H_2$) and the 2- aminophenoxyl radical (**III**-$H_2$).

By photoreduction the parent molecule (a diketone), in an electronically excited

$$\mathrm{RCOCOR} \xrightarrow{h\nu} [\mathrm{RCOCOR}]^*$$

$$[\mathrm{RCOCOR}]^* + \mathrm{R'H} \rightarrow \mathrm{RCO\dot{C}OHR} + \mathrm{R'}\cdot \qquad (2)$$

state (triplet), reacts with a solvent molecule with H-atom abstraction *(equ. 2).*

Photoreduction has been applied for the generation of the 2-hydroxyethenyloxyl radical H–C(O·)=C(OH)–H (**IV**-H), the acetoin radical $CH_3-CO-\dot{C}(OH)-CH_3$ (**V**-H) and the benzoin radical $C_6H_5-CO-\dot{C}(OH)-C_6H_5$ (**VI**-H).

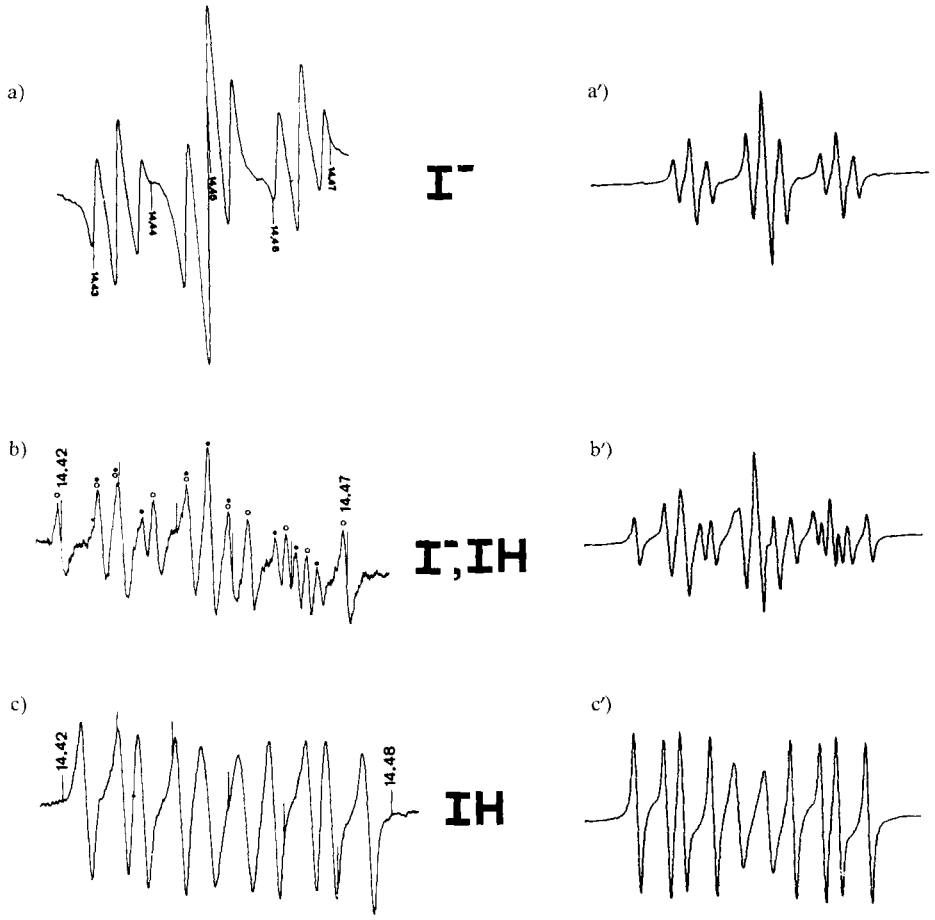


Fig. 1. *Influence of base on the ESR. spectrum of* o-*semibenzoquinone radical in aprotic solvents. Left:* experimental spectra in $CCl_4$/dioxane (0.2M dioxane); concentration of pyrocatechol: $10^{-2}$M; T: 22°. a) With 0.1M triethylamine. b) With $4.4 \cdot 10^{-4}$M triethylamine; circles: lines arising from **I**-H; dots: lines arising from $I^-$ *(cf. Scheme 2).* c) Pure solvent. Marker pips: proton magnetic resonance magnetometer (frequencies given in MHz). *Right:* model calculations based on the kinetic scheme shown in *Scheme 2 (left)* for various populations and protonation-deprotonation rates of radicals derived from **I**-$H_2$. The coupling constants used for the calculations were taken from [14] and *Table 1.* a') Populations: 0.05 for **I**-H and 0.9 for $I^-$, $k = 2.0 \times 10^8\ s^{-1}$, $k' = 6.2 \times 10^5\ s^{-1}$, $k'' = 7.7 \times 10^5\ s^{-1}$. b') Populations: 0.35 for **I**-H and 0.3 for $I^-$, $k$, $k'$ and $k''$ as in a'). The rate constants $k'$ and $k''$ in a) and b) represent the upper limits. c') Populations: 0.5 for **I**-H and 0 for $I^-$, $k = 2.0 \times 10^8\ s^{-1}$; it has been assumed that no intermolecular proton exchange is taking place.

In the indirect photooxidation the first step consists in the photodissociation of di-*t*-

$$(t\text{-BuO})_2 \xrightarrow{h\nu} 2\ t\text{-BuO}\cdot$$

$$t\text{-BuO}\cdot + \text{ArOH} \rightarrow t\text{-BuOH} + \text{ArO}\cdot \qquad (3)$$

butyl peroxide. The *t*-butoxyl radical thus formed abstracts a H-atom from the phenolic parent compound. As a rule, the above method gave rise to the same ESR. spectra as the direct photolysis, but was clearly superior with respect to signal intensity, so was preferred to have optimum spectra in the case of radicals **I**-H, **II**-H and **III**-$H_2$.

**3. Results.** – 3.1. *Photolysis of pyrocatechol* (**I**-$H_2$). The left part of *Figure 1* shows spectra obtained by direct photolysis of **I**-$H_2$ under various conditions. Spectra 1a–1c illustrate the effects obtained by adding base to an aprotic solvent mixture. The photochemical reaction is illustrated in *Scheme 2 (left).*

3.2. *Photolysis of 4-methylpyrocatechol* (**II**-$H_2$). The temperature dependence of the ESR. spectrum of 2-hydroxy-4-methylphenoxyl radical (**II**-H) in an aprotic

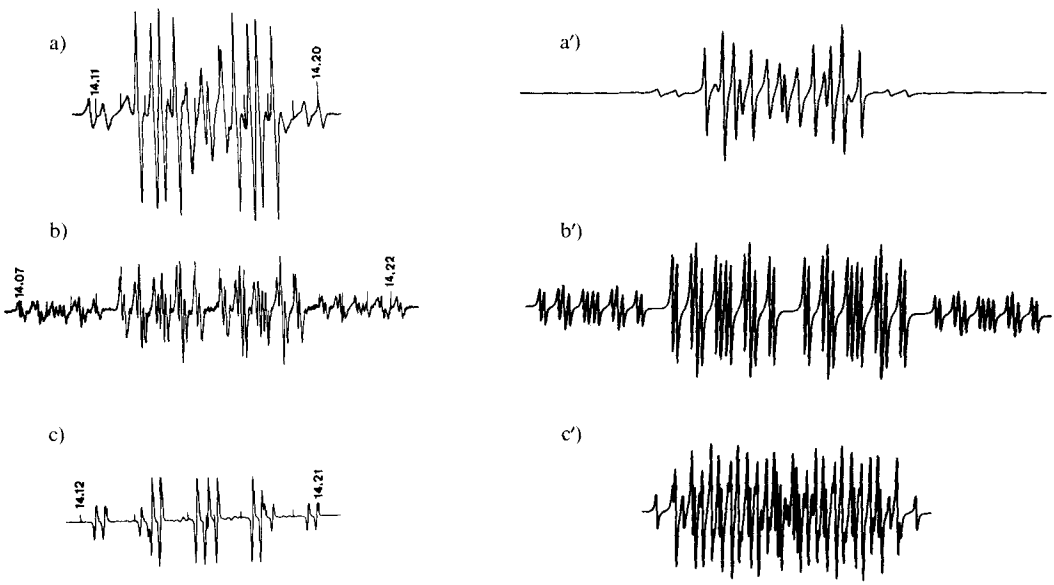


Fig. 2. *ESR. spectra obtained by photolysis of 4-methylpyrocatechol* (**II**-$H_2$). *Left:* experimental spectra; concentration of **II**-$H_2$: $4.0\times10^{-3}$M. a) In $CCl_4$/dioxane (0.2M dioxane), T = 55°. b) In $CH_2Cl_2$/dioxane (0.2M dioxane), T = −74°. c) In methanol, T = 22°. Marker pips: proton magnetic resonance magnetometer (frequencies given in MHz). *Right:* model calculations for the intramolecular hydrogen transfer in radical **II**-H based on the kinetic scheme shown in *Scheme 2 (right).* a') Proton transfer between **II**-H (2L, 2R) and **II**-H (1L, 1R). Populations: **II**-H (2L, 2R) = 0.55; **II**-H (1L, 1R) = 0.45; $k' = 8.0\times10^{-7}$ s$^{-1}$; $k'' = 6.5\times10^{7}$ s$^{-1}$. b') Pure **II**-H (2L, 2R). c') Pure **II**-H (1L, 1R). For the coupling constants used *cf. Table 3.*

Scheme 2. *Intermolecular and intramolecular proton transfer processes for radicals derived from pyrocatechol* (**I**-$H_2$) *and 4-methylpyrocatechol* (**II**-$H_2$) *by photooxidation. Left:* relevant kinetic scheme for the radicals derived from **I**-$H_2$. **I**-H: 2-hydroxyphenoxy radical; $I^-$: conjugate base of **I**-H (anion); $I\text{-}H_2^+$: conjugate acid of **I**-H (cation). *Right:* relevant kinetic scheme for the radicals derived from **II**-$H_2$. The top figure gives the coordinate system and the numbering of the protons at different substitutional and rotameric sites. **II**-H: 2-hydroxy-4-methylphenoxyl; $II^-$: conjugate base of **II**-H (anion).

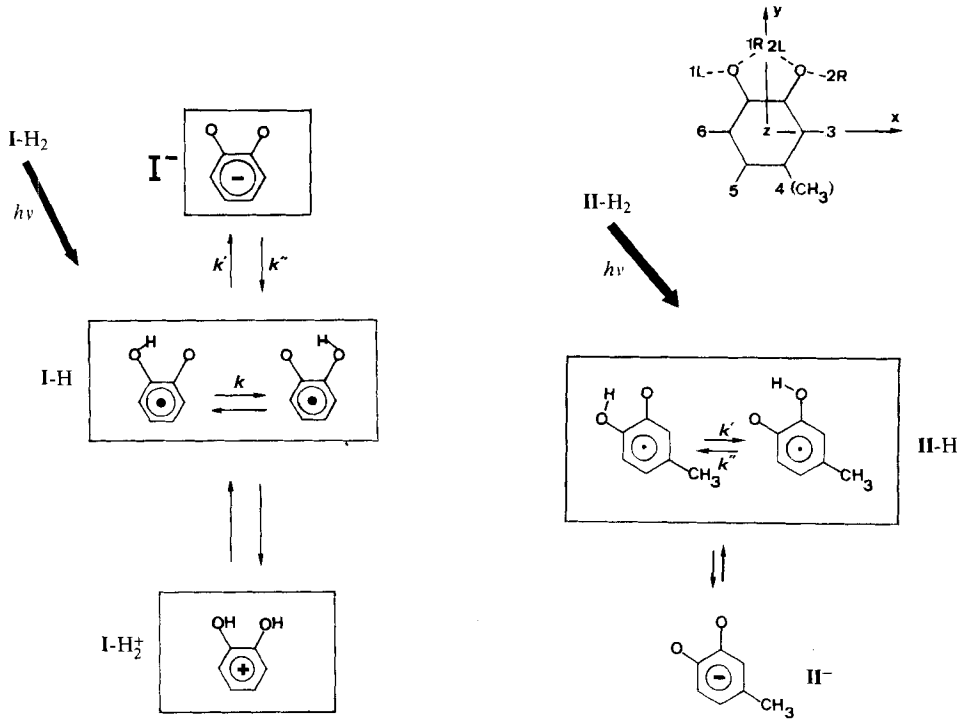


solvent mixture is shown in *Figure 2a* (left part). Conversely, the spectrum of $II^-$, the conjugate radical anion of **II**-H, in methanol demonstrates the solvent dependence of the photochemical reaction *(cf. Fig. 8)*. The coupling constants of the radicals **II**-H and $II^-$ are given in *Table 1*.

3.3. *Photolysis of 2-aminophenol* (**III**-$H_3$). The temperature dependence of the ESR. spectrum of the radical **III**-$H_2$ (obtained by photooxidation from **III**-$H_3$ in an aprotic solvent mixture) and in methanol is shown in *Figure 3* (respectively left and right part). In this case, unlike the two previous cases, addition of base in low concentrations to an aprotic solvent does not yield the same spectrum as in pure methanol. Coupling constants associated with the radical **III**-$H_2$ derived from aminophenol at low temperatures are listed in *Table 2* (also compare *Fig. 7*).

3.4. *Photoreduction of diacetyl* (**V**) *in H-donating solvents.* The spectra obtained by photolyzing **V** in toluene at $-69°$ is shown in *Figure 4a*. The coupling constants obtained for the 3-hydroxy-2-butenyl-2-oxyl radical (**V**-H) derived from **V** *(cf. Fig. 6)* under different conditions of temperature and solvent are given in *Table 1*.

Table 1. *Experimental coupling constants* (in gauss, absolute values) *for radicals derived from* **I**-$H_2$, **II**-$H_2$, **IV**, **V** *and* **VI**

| Radical | Solvent | Temp. | Ref. | Position | | | | | |
|---|---|---|---|---|---|---|---|---|---|
| | | | | 1 | 2 | 3 | 4 | 5 | 6 |
| **I**[-a]) | $H_2O$ | RT. | [31] | | | 0.77 | 3.75 | 3.75 | 0.77 |
| | $H_2O$ | RT. | [32] | | | 0.75 | 3.75 | 3.75 | 0.75 |
| | $H_2O$ | 22° | This work | | | 0.73 | 3.72 | 3.72 | 0.73 |
| | $CH_3OH$ | 22° | This work | | | 0.61 | 3.82 | 3.82 | 0.61 |
| | $CH_2Cl_2/CH_3CN/NEt_3$ | 22° | This work | | | 1.14 | 3.52 | 3.52 | 1.14 |
| | $CCl_4$/dioxane/$NEt_3$ | 22° | This work | | | 0.9 | 3.64 | 3.64 | 0.9 |
| **II**-H[a]) | $CH_2Cl_2$/dioxane | −74° | This work | 1.35 | | 1.84 | 9.68 | 0.38 | 3.89 |
| **II**[-a]) | $CH_3OH$ | 22° | This work | | | 0.1 | 5.00 | 3.98 | 0.77 |
| **IV**-H-*cis*[b]) | Toluene | 20° | [18] | 18.0 | 3.0 | 1.1 | | | |
| | Toluene | −34° | [18] | 17.9 | 3.0 | 1.2 | | | |
| **IV**-H-*trans*[b]) | Toluene | −34 | [18] | 14.9 | 4.0 | 2.9 | | | |
| | Toluene | −102° | [18] | 14.9 | 4.0 | 3.0 | | | |
| **V**-H[b]) | Toluene | 94° | This work | 15.07 | 1.24 | 1.24 | | | |
| | Toluene | 30° | This work | 14.8 | 1.39 | 1.75 | | | |
| | Toluene | −69° | This work | 14.4 | 1.9 | 2.38 | | | |
| | $CCl_4$/toluene | 22° | This work | 14.8 | 1.4 | 1.75 | | | |
| | $CH_2Cl_2/CH_3CN$ | 22° | This work | 14.5 | 1.86 | 1.86 | | | |
| | $CH_3OH$/toluene | 22° | This work | 13.9 | 2.8 | 2.2 | | | |
| | 2-Propanol | | [25] | 13.41 | 2.58 | 2.07 | | | |
| **VI**[-c]) | $CH_3OH$/toluene | 22° | This work | 1.43 | 0.48 | 1.47 | | | |
| | Dimethylformamide | | [27] | 0.99 | 0.36 | 1.12 | | | |

[a]) The numbering refers to the top figure of *Scheme 2 (right)*. [b]) The numbering refers to *Scheme 3*. [c]) The numbering 1, 2 and 3 refers to the *o*-, *m*- and *p*-position in the benzene rings of the benzil anion (**VI**$^-$).

3.5. *Photoreduction of benzil* (**VI**). *Figure 5a* shows the ESR. spectrum of a solution of **VI** in an aprotic solvent photolyzed at RT. *Figure 5b* illustrates the kind of spectra obtained when a mixture of toluene and methanol is used. Coupling constants for the radical anion **VI**$^-$ obtained in methanol/toluene are presented in *Table 1*.

**4. Discussion.** – 4.1. *Proton exchange across symmetric and asymmetric potentials.* For sake of clarity we will start from the case where the intramolecular proton transfer corresponds to the motion in a double minimum potential along one reaction coordinate Q. This situation is visualized in *Figure 6a*, were the potential function $V(Q)$, with two minima at $Q_A$ and $Q_B$ is associated with the localized structures (sites) A and B, respectively. In the language of chemical exchange *(cf. Fig. 6b)* this corresponds to the case with two sites A and B with resonances frequencies $\omega_A$ and $\omega_B$ and spin jumping between the sites at rates $k_{AB}$ and $k_{BA}$, respectively. With $\Delta G \approx \Delta V$ the equilibrium constant is given by *equ. 4 (cf. Fig. 6b)*

$$K = \exp(-\Delta V/RT) = f_B/f_A = k_{AB}/k_{BA} \tag{4}$$

*Fig. 6b)* where $\Delta V = E_B^O - E_A^O = V_{AB} - V_{BA}$ is the difference between the vibrational ground states (notation of [15]).

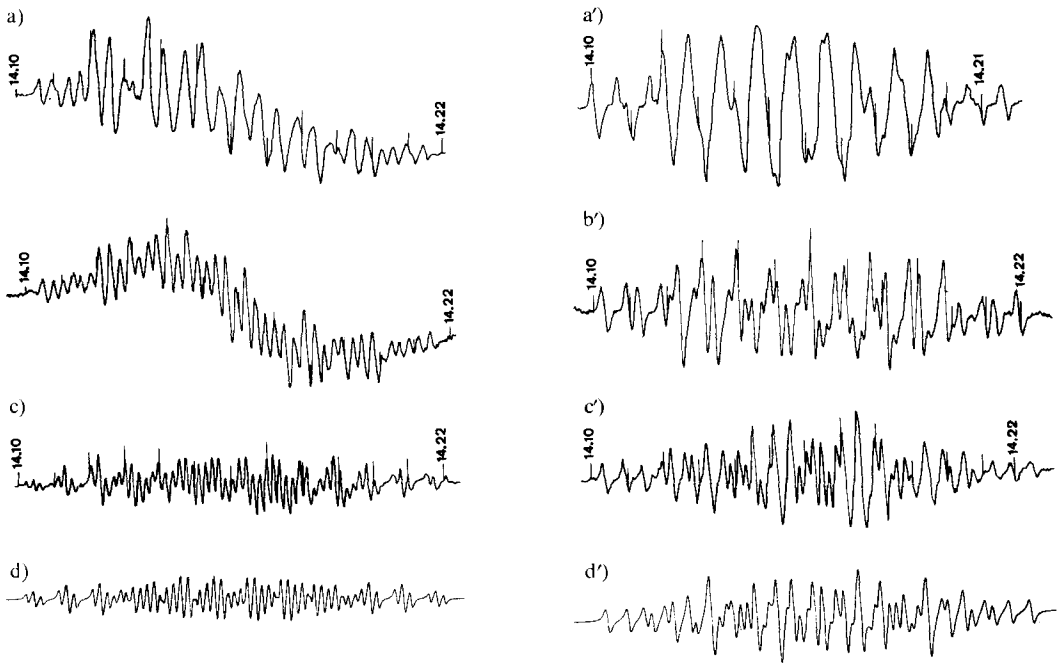


Fig. 3. *ESR. spectra obtained during photolysis of 2-aminophenol* (**III**-$H_3$). *Left:* concentration of **III**-$H_3$: $1.5\times 10^{-2}$M; in $CH_2Cl_2$/tetrahydrofuran (9:1); a) T = 37°; b) T = 22°; c) T = – 61°; d) computer simulated spectrum of c with coupling constants given in *Table 2. Right:* in concentration of **III**-$H_3$: $1.5\times 10^{-2}$M in methanol; a') T = 55°; b') T = 22°; c') T = – 75°; d') computer simulated spectrum of c' with coupling constants given in *Table 2.* Marker pips: proton magnetic resonance magnetometer (frequencies given in MHz).

Table 2. *Experimental coupling constants* (in gauss, absolute values) *for 2-aminophenoxyl* (**III**-$H_2$). The numbering refers to *Figure 7.*

| Temp. | Solvent | Ref. | Position | | | | | | |
|---|---|---|---|---|---|---|---|---|---|
| | | | H' | H'' | 3 | 4 | 5 | 6 | N |
| – 61° | $CH_2Cl_2$/tetrahydrofuran | This work | 7.6 | 5.8 | 0.46 | 2.25 | 0.53 | 2.18 | 4.43 |
| – 75° | $CH_3OH$ | This work | 6.9 | 5.5 | 0.1 | 3.0 | 1.4 | 2.5 | 4.5 |
| RT. | $H_2O$ | [20] | 5.3 | 5.3 | 0.1 | 4.31 | 1.01 | 2.94 | 4.76 |
| RT. | $H_2O$ | [21] | 8.13 | 8.13 | 0.9 | 6.62 | 1.5 | 2.6 | 6.62 |

Furthermore, if we assume that the intramolecular potential barrier is a good estimate for the energy of activation of the proton transfer process and that $\mathrm{sgn}(V_{AB}) = \mathrm{sgn}(V_{BA}) = +1$, we can use the *Arrhenius* equation in the form 5 (for the forward and backward reactions).

$$k_{AB} = A \exp(-V_{AB}/RT) \qquad k_{BA} = A \exp(-V_{BA}/RT) \tag{5}$$

Whereas one can in general approximate the barrier to interconversion from the minimum of the electronic potential curve, such as in the case of the internal

Table 3. *INDO- and experimental coupling constants for the tautomeric forms of radical* **II**-H. The numbering and the position of the hydroxylic proton refers to the top figure of *Scheme 2 (right)*. The coupling constants in parenthesis have been used for the model calculation in *Figure 2*. Tautomer 2L corresponds to 2-hydroxy-4-methylphenoxyl, whereas the tautomer 1R is 2-hydroxy-5-methylphenoxyl if the frame is kept fixed as in our *Table*. The coupling constants of radical 1R given in parenthesis are those determined by a fitting procedure *(cf. Fig. 2)*. The corresponding coupling constants for the radical 2L are those determined directly from the low temperature spectrum and are identical to those given in *Table 1*.

| Tautomer of **II**-H | Position | | | | | |
|---|---|---|---|---|---|---|
| | 1R | 2L | 3 | 4 | 5 | 6 |
| 2L | | −0.4<br>(−1.35) | 2.18<br>(1.84) | 4.58<br>(9.68) | 2.18<br>(0.38) | −4.1<br>(−3.89) |
| 1R | −0.5<br>(−1.19) | | −4.16<br>(−4.02) | −2.95<br>(−1.39) | −3.57<br>(−7.62) | 2.16<br>(1.94) |

Scheme 3. *Representative kinetic graph for the intramolecular dynamic processes in radicals derived from* **IV**, **V** *and* **VI**. The top figure gives the numbering of the protons. Conformers are labelled as l and r depending on the H(3) with respect to the molecular *yz*-plane (only the l-branch is shown), whereas o or c denotes the rotamers obtained by opening or closing the intramolecular H-bond. Finally *cis* or *trans* are defined as usual with respect to the conformation of the OCCO frame. **IV**-H: R = H, **V**-H: R = $CH_3$, **VI**-H: R = phenyl.

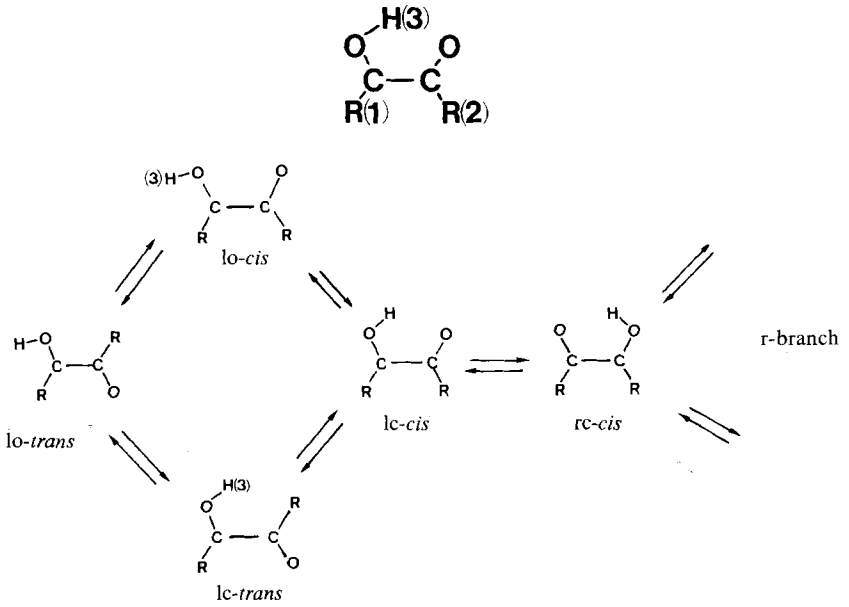


rotation of a phenyl group, it is of importance for the intramolecular proton transfer, to take into account specifically the zero-point vibrational energy $E_A^O$ and $E_B^O$ associated with the coordinate Q [16]. For a proton which oscillates in a O–H···O bridge, the zero-point energy of the stretching vibration may amount to

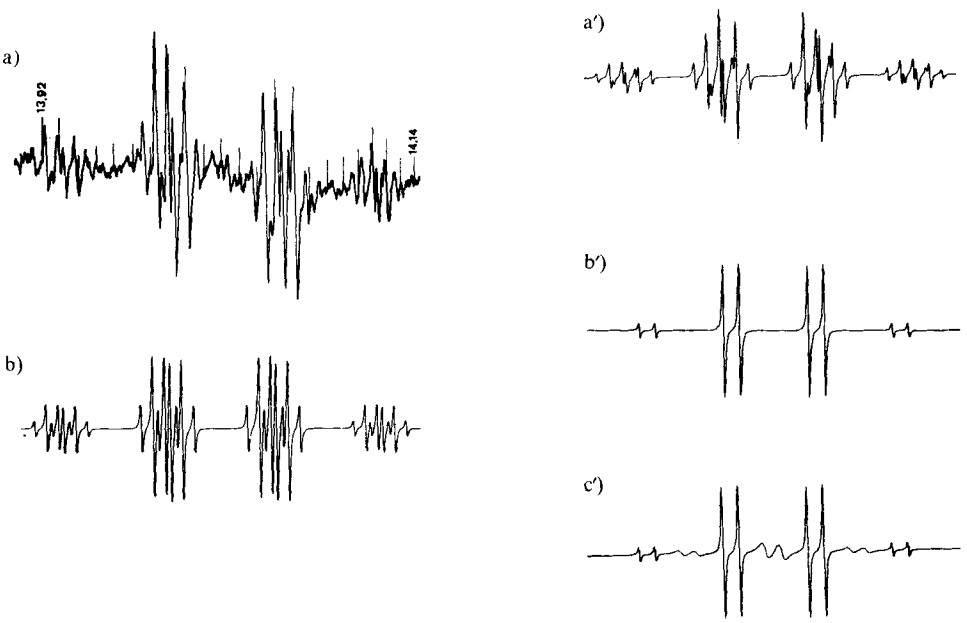


Fig. 4. *ESR. spectra obtained during photolysis of a solution of biacetyl* (**V**). *Left:* experimental and computer simulated spectra for the 3-hydroxybut-2-enyl-2-oxy radical (**V-H**). Solvent: toluene, concentration of **V**: $3.3\times 10^{-2}$ M; a) $T=-69°$; b) computer simulated spectrum with coupling constants given in *Table 1. Right:* computer simulated spectra in the assumption of an intramolecular hydrogen transfer (1c-*cis* ⇄ rc-*cis*) as depicted in *Scheme 3.* Coupling constants used for the calculation, *cf. Table 1.* The following rate constants of the intramolecular hydrogen transfer were used: a') $k=1.4\times 10^5$ s$^{-1}$; b') $k=1.4\times 10^7$ s$^{-1}$; c') $k=1.4\times 10^9$ s$^{-1}$.

about 5 kcal/mol, which is of the same order of magnitude as the barrier $V_{AB}$ in many cases. This very high zero point energy is the reason why the intramolecular proton exchange is often too fast to be studied by NMR. With respect to the shape of the potential curve the following distinction applies.

(i) Symmetric potential ($\Delta V=0$). This is obviously realized when A and B are two symmetrically equivalent structures. The best known cases of intramolecular proton transfer belong to this class, including the naphthazarin anion which is an example of very fast tautomerism. Neither exchange rates nor a barrier were obtained for it by ESR. [17]. Symmetrically substituted *o*-semibenzoquinones, on the other hand, show intermediate exchange rates where the barriers can be obtained with high accuracy from ESR. measurements [11]. Finally, in the 2-hydroxy-ethenyloxyl radical CHOH=CHO· obtained by photoreduction of glyoxal in aprotic solvents the proton transfer across the O–H...O bond is too slow to be detected by ESR. spectroscopy [18]. The analytical expressions for the extra-line broadening due to exchange $1/T_{2ex}$) are readily obtained from [15] with $k_{AB}=k_{BA}=k$, when:

for slow exchange ($k \ll |\omega_A-\omega_B|$), $\quad 1/T_{2ex}=k$ (6)

for fast exchange ($k \gg |\omega_A-\omega_B|$), $\quad 1/T_{2ex}=1/8k\,(\omega_A-\omega_B)^2$ (7)

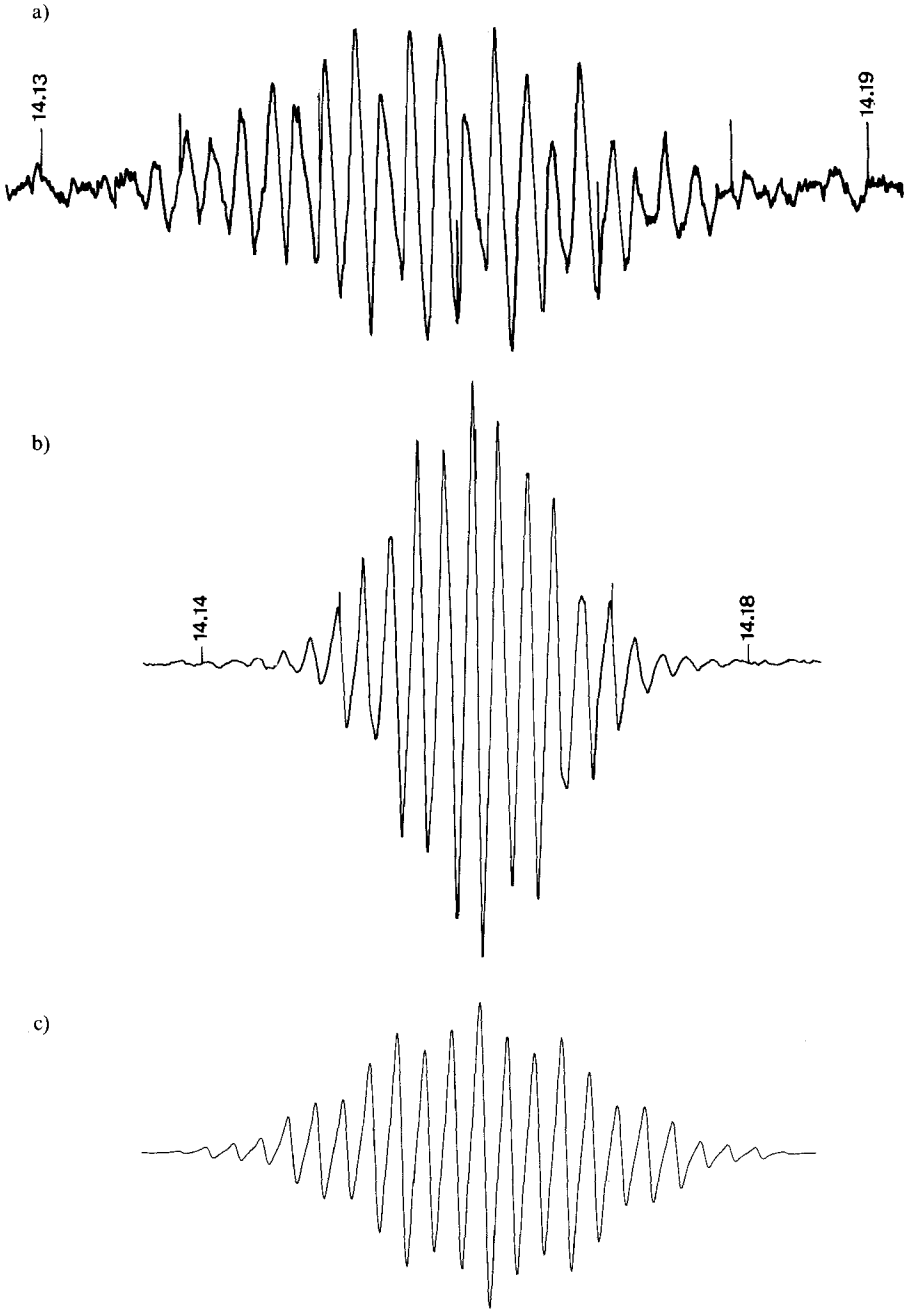


Fig. 5. *ESR. spectra obtained during photolysis of benzil* (**VI**). a) Solvent: $CCl_4$/dioxane/pentane 8:1:1, concentration of **VI**: $7.6\times 10^{-3}$ M; T = 22°. b) Solvent: methanol/toluene 10:1, concentration of **VI**: $7.8\times 10^{-3}$ M; T = 22°. c) Computer simulated spectrum of b with coupling constants given in *Table 1*. Marker pips: proton magnetic resonance magnetometer (frequencies given in MHz).

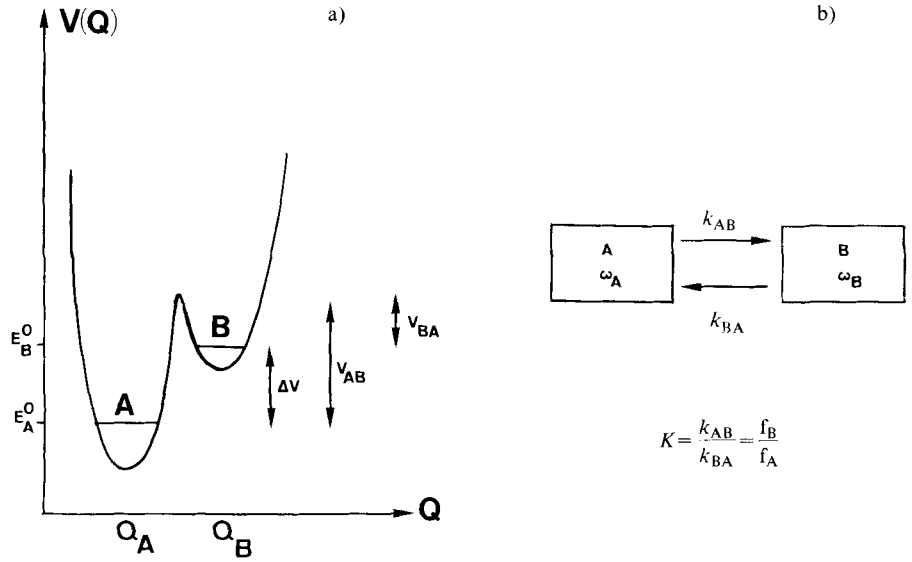


Fig. 6. *General proton exchange potential and dynamics.* a) Electronic double minimum potential energy curve $V(Q)$. $Q_A$ and $Q_B$ represent two tautomeric forms differing in energy by an amount $\Delta V$ and separated by a potential barrier $V_{AB}$ and $V_{BA}$ taken with respect to the lowest stretching vibrational levels. b) Corresponding kinetic scheme for a simple exchange process. $k_{AB}$ and $k_{BA}$ are the jumping rates between the distinct sites A and B. $K$ is the equilibrium constant for the reversible process (*cf.* section 4.1), and $f_A$ and $f_B$ are the fractional populations of the sites A and B respectively.

These equations allow straightforward determination of the exchange rate in favourable cases [4].

(ii) Asymmetric potential ($\Delta V \neq 0$). If A and B are inequivalent structures, then the potential $V(Q)$ is not any longer symmetrical and $\Delta V$ is not zero. In the following, we will assume without loss of generality, that $f_A$, the fractional population associated with the site A, is the larger of the two.

When $\Delta V \approx V_{AB}$ is too large ($\Delta V \geq 10$ kcal/mol, see also sect. 4.1.2) there is no measurerable effect from tautomeric forms other than A on the ESR. spectrum, as illustrated by 2,6-dihydroxyphenoxyl [11].

Wen the difference in energy between the two tautomers, $\Delta V$, is of the order of 2 kcal/mol and smaller than $V_{AB}$ we do observe kinetic effects on the ESR. spectrum (*cf.* sect. 4.1.1). For the equilibrium constant it follows that at RT., $\exp(-\Delta V/RT) = K \leqslant 3 \cdot 10^{-2}$ which implies that $f_a \approx 1$ and $k_{BA} \gg k_{AB}$. For the extra line broadening, $1/T_{2ex}$, for the limiting case of an asymmetric potential

for slow exchange ($k_{AB}, k_{BA} \ll |\omega_A - \omega_B|$), $\quad 1/T_{2ex} = K \cdot k_{BA}$ (8)

for fast exchange ($k_{AB}, k_{BA} \gg |\omega_A - \omega_B|$), $\quad 1/T_{2ex} = (\omega_A - \omega_B)^2 \cdot K/k_{BA}$ (9)

($\Delta V \geq 1$ kcal/mol). *Equations 8* and *9* are very similar to those for the symmetric case, *equations 6* and *7*. This means that in a sufficiently asymmetric case the

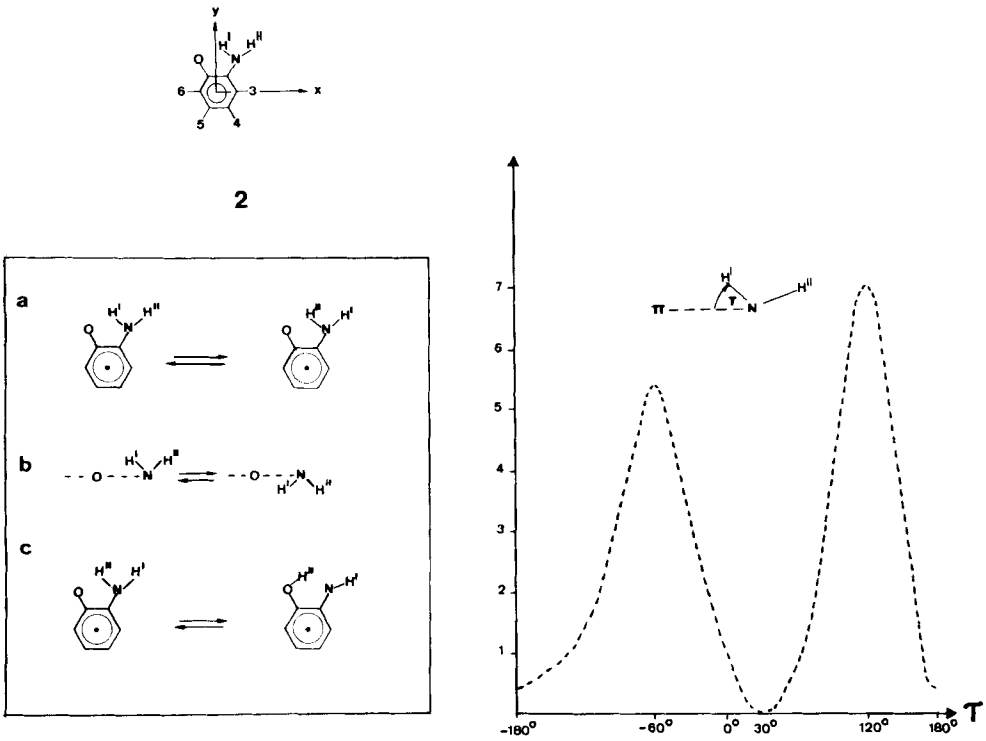


Fig. 7. *Kinetic graph for the relevant intramolecular motions in 2-aminophenoxyl* (**III**-$H_2$) *and the potential for the rotation of the amino group. Left:* the top figure gives the numbering of the protons and the molecular coordinate system. In the box three different types of intramolecular dynamics are shown. a) Internal rotation of the amino group in the case of $sp^2$-hybridization. This would correspond to an exchange of the protons H′ and H″. b) Inversion at the $sp^3$-hybridized nitrogen. This process does not interchange the hyperfine splittings of the substituents H′ and H″ and therefore can not be detected by dynamic ESR. spectroscopy. c) Intramolecular proton transfer connecting the phenoxy and the amino type tautomers of radical **III**-$H_2$. *Right:* INDO-potential curve for the rotation of an $sp^3$-hybridized amino group in 2-aminophenoxyl, using standard bond length and bond angles [22] [35]. The relative energy $\Delta E$ is given in kcal/mol. In the energy minimum arrangement of the intramolecular O···H–N hydrogen bond the bridge proton does not lie in the ring plane with N and O.

observed exchange-line broadening is not directly related to a rate constant as in the symmetric case, but is also dependent on an equilibrium constant. One should therefore exercize due care in the data analysis if activation energies are determined from a temperature dependent study. In the case of slow exchange one might observe the broadening of a line of A as a function of increasing temperature. Inserting *equations 4* and *5* into expression 8 one obtains *equation 10*

$$1/T_{2ex} = K \cdot k_{BA} = A \cdot K \cdot \exp(\Delta V/RT) \cdot \exp(-V_{AB}/RT) = A \cdot \exp(-V_{AB}/RT) \quad (10)$$

because $-V_{BA} = \Delta V - V_{AB}$, and hence the activation energy determined by the regression of $1/T_{2ex}$ *vs.* $1/T$ is that of the foreward process A → B. The equilibrium constant $K$ itself is measured by the ratio $S_B/S_A$ of the (integral) signals due to A and B in the

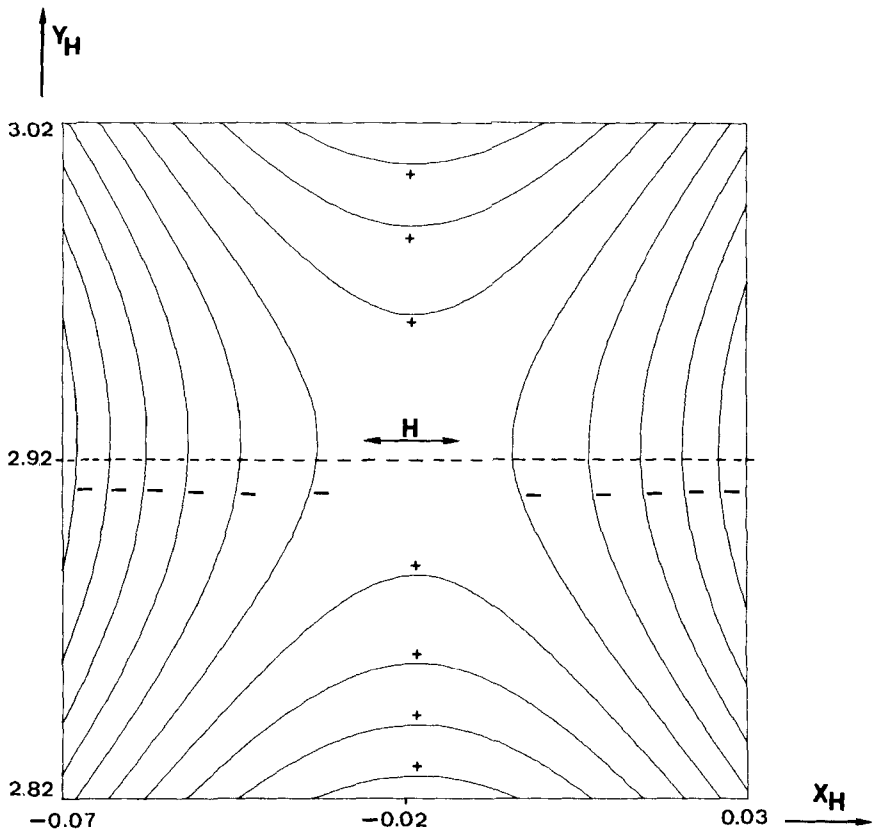


Fig. 8. *Potential surface in the near of the transition state for the proton transfer 1R ⇌ 2L in the radical* **II**-H. The coordinate system is given in the top figure of *Scheme 2*, the transition state has been determined from an INDO calculation. The coordinates of the hydroxylic proton in the partially optimized state are $x_H = -0.02$ Å and $y_H = 2.92$ Å, as determined from a regression analysis of the function $E(x_H, y_H) = a + bx_H + cy_H + dx_H^2 + ex_Hy_H + fy_H^2$. The energy difference between two lines is 0.4 kcal/mol. The path followed by the hydroxylic proton during a proton transfer between the two oxygen atoms is approximatively given by the broken line which is orthogonal to the equipotential lines. Levels of increasing (decreasing) energy with respect to the transition state are labeled by + ( − ).

absence of exchange. With fast or intermediate exchange, however, it is not any longer possible to assign a certain line of the spectrum to A or B, and therefore $K$ cannot be determined independently. One may try to slow down the exchange process, but this is not the solution to the problem because decreasing the temperature can lower the fractional population of the less stable tautomer below the level of detection. Furthermore, the exchange process may be fast even at temperatures where $f_B \ll f_A$, in which case *equation 9* applies. In addition to the equilibrium constant $K$, not directly obtainable, one needs also the complete set of coupling constants for site B, which cannot be directly determined either. This very case was encountered with radical **II**-H (*cf.* sect. 4.1.1). The data can therefore only be extracted from the spectra by means of an extensive fitting procedure [34], where the starting

data set should already be more accurate than obtained by current quantum chemical methods.

(iii) Proton exchange in the presence of additional intramolecular dynamic processes. In few cases only does the intramolecular proton exchange (symmetrical or not) take place along a one-dimensional reaction coordinate (as *e.g.* proton tautomerism in porphyrins). Generally, we found that further, often unexpected, intramolecular degrees of freedom, such as internal rotation and inversion, interfere with the proper proton transfer leading to complex, multi-site exchange problems (*cf.* sect. 4.2). Considering the difficulties mentioned above and the solvent effects to be discussed later, we would claim that *e.g.* the aminophenoxyl radical (**III**-$H_2$, *cf.* sect. 4.1.2) is at the limit of interpretability for the present state of the art of spectroscopic and quantum chemical techniques.

4.1.1. *Weakly asymmetric potential. The effect of methyl substitution on structure and dynamics in the 2-hydroxy-4-methylphenoxyl radical* (**II**-H). The ESR. spectrum of **II**-H is strongly temperature dependent and characterized by a wide pattern at low temperatures ($T \leqslant = 74°$) which narrows steadily as the temperature increases. As for the parent radical **I**-H, we find that this type of temperature dependence arises from the intramolecular proton transfer as schematized in *Scheme 2*. From the low temperature spectrum a complete set of proton hyperfine splittings (including that for the hydroxylic proton) is obtained *(cf. Table 1)*. However, it is not *a priori* clear to which of the 4 possible structures 1L, 1R, 2L and 2R *(cf. Scheme 2 (right))* this set has to be assigned. An INDO calculation analogous to that for **I**-H (*cf.* [11]) shows that within a few kcal/mol all four possible rotamers and protomers have the same energy, which precludes any reliable conclusion. The barrier to interconversion between the sites 1R and 2L, $V_{AB}$, is found by INDO to be of the order of 20 kcal/mol in close agreement to the result obtained for **I**-H [11]. In contrast to the case of 2-hydroxyphenoxyl (**I**-H), where the transition state can be assumed to have symmetry $C_{2v}$, no such restriction can be imposed on the transition state connecting 1R and 2L of radical **II**-H. For this calculation the transition state geometry of **I**-H has been used as a frame [11] in which only the coordinates of the hydroxylic proton $x_H$ and $y_H$ were varied. The calculated points were fitted to a surface of second order from which the coordinates of the saddle point were determined (*cf.* key of *Fig. 8*). A more complete analysis of the rate process $1R \rightleftarrows 2L$ should indicate how the slight asymmetry of the transition state is reflected in a difference between the kinetic parameters of the forward and backward reaction, *i.e.* $A_{AB} \neq A_{BA}$ and $V_{AB} \neq V_{BA}$.

The rotamers 2R and 1L may be ruled out in the first approximation since they do not allow the formation of an intramolecular hydrogen bond and in the case of **I**-H they only affected the line width to a minor extent [11]. The two protomers 1R and 2L can be differentiated by means of their significantly different spin density distributions [11] [19]. Structure 2L corresponds to a 2-hydroxy-4-methylphenoxyl radical, for which a large *p*-methyl hyperfine splitting a ($CH_3$) is expected, whereas 1R corresponds to a 2-hydroxy-5-methylphenoxyl radical with the methyl group in the *m*-position and a very small spin density on it. These qualitative predictions about the spin densities are fully confirmed by INDO calculations, so that one

concludes that the *p*-methyl structure, which is indeed observed at low temperatures, is the more stable. At higher temperatures, as the *m*-methyl structure with its smaller total splitting is increasingly populated, we observe an apparent narrowing of the ESR. spectrum. This model allowed for a satisfactory interpretation of the ESR. spectrum *(cf. Fig. 2)*.

4.1.2. *Strongly asymmetric potential. Tautomerism and dynamics in the* o-*aminophenoxyl radical* (**III**-$H_2$). The low temperature spectrum ($T < -60°$) obtained by irradiation of a solution of *o*-aminophenol in an aprotic solvent *(cf. Fig. 3,* spectrum c) leads to a set of hyperfine splitting constants, which can be fitted to the expected 2-aminophenoxyl radical *(cf. Table 2)*. This radical has been previously postulated by *Neta et al.* [20] and the hyperfine constants from their work are also shown in *Table 2*. The two sets of values show obvious discrepancies, in particular, in our case two different couplings are assigned to the protons of the amino substituent. Based on the strong temperature dependence of the ESR. spectrum in an aprotic solvent it is suggested that the two amino protons may be involved in an intramolecular dynamic process *(cf. Fig. 3)*. Closer comparison with the data obtained by *Neta et al.* is complicated by the fact that the ESR. spectrum of **III**-$H_2$ is not only dependent on temperature but also strongly on solvent (a spectrum of aminophenoxyl in methanol leads to other hyperfine values than in water). *Dixon et al.* [21] have also obtained a spectrum of 2-aminophenoxyl but choose a different assignment of coupling constants *(Table 2)*. Whereas the solvent dependence will be dealt with more generally in a subsequent section, we shall discuss the possible dynamic processes of *o*-aminophenoxyl as follows. Radical **III**-$H_2$ exhibits an intramolecular H-bond between an O- and a N-atom. *A priori*, two possible non-equivalent tautomeric structures have to be considered, O–H···N and O···H–N, which have different stabilities. A simple INDO calculation confirms the chemical intuition that the proton is covalently bonded to the stronger acceptor, the N-atom, and that the energy difference $\Delta V$ is very large, of the order of 20 kcal/mol. This rules out the O–H···N structure in any kind of thermodynamic and kinetic considerations, in agreement with previous work [20]. In order to gain insight in the intramolecular potentials governing the dynamic processes a limited number of points of the relevant potential surface were calculated with the help of an INDO program [22].

First, it turned out that the amino group in *o*-aminophenoxyl is probably not planar, but at least partially $sp^3$-hybridized. This is in agreement with the structure of the amino group in aniline as determined by microwave measurements [23]. Taking now an $sp^3$-hybridized N-atom, the amino group was rotated around the CN axis by an angle $\tau$ yielding the potential shown in *Figure 7*. The curve $V(\tau)$ exhibits a minimum at $\tau \cong 30°$ and two maxima at $\tau \cong -60°$ and $\tau \cong 120°$ characterized by barriers of 5 and 7 kcal/mol, respectively. That the energy minimum does not occur at $\tau = 0°$ suggests that the O···H–N bond does not lie necessarily in the aromatic ring plane. Over the whole domain of the angle $\tau$ the N-atom splitting remains confined to smaller values a(nN) ($\leq 1$ gauss) than the experimental one *(cf. Table 2)*. As the final step in geometry optimization, out-of-plane deformation of the radical caused by bending of the C,N-bond out of the *xy*-

plane of the ring was considered *(cf. Fig. 7)*. This deformation further stabilizes the energy by at least 5 kcal/mol at an optimum value of the bending angle of about 5°. The coupling constant of the N-atom increases thereby significantly and reaches a value of approximately 3 gauss, which now compares more favourably with the experimental one. We are perfectly aware of how questionable results obtained by a partial geometry optimization method actually are. However, since (i) the temperature dependence of the ESR. spectrum is experimentally well documented, and (ii) an intramolecular proton transfer can be excluded under our experimental conditions, the internal rotation of the amino group, possibly accompanied by other bending and/or inversion motions *(cf. Fig. 7)* appears as the likely cause for this temperature dependence.

The complete analysis of the ESR. line shape is also complicated by the temperature dependence of the hyperfine constants themselves and has not yet been carried out. Despite efforts in this direction it was not possible to obtain reasonable estimates of the coupling constants with INDO, a problem which has already been mentioned [21]. As can be seen from *Table 2,* in which experimental coupling constants from three independent sources are reported, agreement in the assignment is still missing.

4.2. *Steric effects and the stability of intramolecular H-bonds.* In this section we present radicals produced by photolysis of glyoxal (**IV**), biacetyl (**V**) and benzil (**VI**), which have structures where rotation around the C, C-bond of a HO–C–C–O fragment is allowed. Consequently, two conformations are possible for such a radical, a *cis*-type, in which the closing of the O–H···O bond is geometrically feasible, and a *trans*-type, which precludes the formation of an intramolecular H-bond. The relative energy of the two *cis* and *trans* conformations as shown in *Scheme 3* is obviously dependent on a large number of intramolecular potentials, but, in a simple picture, it can be viewed as reflecting the balance between the stabilization due to the formation of an intramolecular H-bond and the destabilization due to the repulsion of the two substituents R at the C, C-bond in the *cis*-configuration.

Irradiation of **IV** in toluene leads to an ESR. spectrum, which is temperature dependent and consists of three independent sub-spectra. Two of these sub-spectra are due to the expected radical HO–ĊH–CH=O (**IV**-H), one for the *trans* the other for the *cis*-form. Thorough analysis of the temperature dependence of the relative quantum yield showed that the *trans* radical is first formed from the triplet, which then interconverts to the thermodynamically more stable *cis*-form with an internal H-bond. Finer temperature-dependent details of the ESR.-line shape could be satisfatorily explained by assuming hindered rotation of the hydroxyl group and finally the whole analysis was based on an *ab initio* calculation for the relative energies of the structures involved [18]. The main result was that the ESR. spectrum does not yield any information about an intramolecular proton transfer across the O–H...O bridge (process lc⇄rc-*cis*) but rather about *trans-cis* isomerisation (lo-*trans*⇄lo-*cis* and lc-*trans*⇄lc-*cis*) and internal rotation of the hydroxyl group (lo-*cis*⇄lc-*cis* and lo-*trans*⇄lc-*trans (cf. Scheme 3).*

Surprisingly enough, irradiation of biacetyl (**V**) in toluene leads to only one distinguishable ESR. spectrum (*cf. Fig. 4a*, left part). The coupling constants

derived from the spectrum of the 3-hydroxy-2-butenyl-2-oxyl radical (**V-H**) are listed in *Table 1* and show a weak temperature dependence, except for the hydroxylic proton coupling $a^H(3)$. In order to determine the preferred conformation and the relevant dynamic processes in radical **V-H** we first recall that biacetyl (**V**) has a *trans*-conformation not only in the electronic ground state, but also in the first excited triplet state **V*** [24]. The discussion will therefore be based on the

$$\mathbf{V^*}\ (trans) \xrightarrow{\text{H-abstraction}} \mathbf{V\text{-}H}\ (trans) \rightleftharpoons \mathbf{V\text{-}H}\ (cis)$$

following kinetic scheme. Accordingly, radical **V-H** is first formed upon H-abstraction in its *trans*-form, and can consequently interconvert to the *cis*-form. If the barrier of interconversion, found to be about 7 kcal/mol in the case of radical **IV-H** [13] [18][1]), is of this order of magnitude, then we should, as for **IV-H**, observe the *trans*-form at low temperatures (*e.g.* at $-69°$). Increasing the temperature to $+94°$ does not reveal line shift and/or broadening effects as observed for **IV-H**. Therefore we would conclude that no chemical exchange is occurring between a *trans* and a *cis* site of **V-H**. In fact, the temperature dependence of $a^H(3)$ can be accounted for by the torsional oscillation of the C–O–H fragment as shown by *Krusic et al.* [9] in the case of the hydroxymethyl radical $\dot{C}H_2OH$.

INDO calculations also suggest that the *trans*-conformation is the more stable. Using standard structural parameters [35] we found that the difference in total energy *E(trans)–E(cis)* is *ca.* $-1$ kcal/mol, while it was *ca.* $+5$ kcal/mol for radical **IV-H** [13] [18]. The increased steric repulsion in the *cis*-conformation of **V-H** is likely to be responsible for this difference. We also tested the possibility of a contribution of the intramolecular proton exchange, which should occur at sufficiently high temperatures in the *cis*-conformation. A set of spectra were simulated [34] in which the lc-*cis* ⇆ rc-*cis* exchange was varied *(cf. Fig. 4)*. Since even at the highest temperature ($+94°$) no kinetic effect of this kind could be observed in the ESR. line shape, we finally favour the interpretation that the radical **V-H**, which is first formed in its *trans*-form, does not interconvert to the *cis*-form. We should not conceal, however, that from IR. measurements [26] it has been assumed that at RT. the *cis*-form of **V-H** is present. Furthermore, in the case of the semidione radical anion **V**, which is more stable in its *trans*-configuration, it has been postulated that in the presence of $Li^+$ the *cis* form is selectively stabilized by chelation [36].

The photoreduction of benzil in an aprotic solvent leads to the ESR. spectrum in *Figure 5a*, which we tentatively assign to the up to now unknown 1,2-diphenyl-2-hydroxyethenyloxyl radical (**VI-H**). *A priori*, the steric hindrance of the two phenyl groups in the *cis*-conformation should strongly overcompensate the gain in energy obtained by forming the intramolecular H-bond. In fact, the spectrum is temperature independent, which also seems to support the assignment of **VI-H** to the *trans*-form. An indication that the radical obtained by photolysis of benzil is indeed **VI-H**, is

[1]) The authors point out a typing error in [18]: in *Table 1* and *7* the coupling constants $a_5$, $a_6$ and $a_7$ should be read instead of $a_6$, $a_7$ and $a_5$, respectively.

given by the spectrum in *Figure 5b*, obtained by photolyzing **VI** in methanol/toluene (*cf.* sect. 4.3.2). In this basic solvent mixture we obtain a spectrum which is identical to that reported by *Dehl et al.* [27] for the reduction of benzil, and assigned to the anion $\mathbf{VI}^{-\cdot}$.

4.3. *Solvent effects.* Solvent effects on the ESR. spectra of organic radicals have been reported [28], in particular for phenoxyl radicals [29] which are similar to the radicals discussed here. Relative variation of the coupling constants of up to 40% were measured. For the radicals at hand, which are able to form an intramolecular H-bond and an intermolecular one with a solvent molecule, the observed dependence of the hyperfine splitting on variation of solvent often turned out to be as large. If the interaction between the hydroxyl group of the radical and the solvent is strong enough, then proton transfer will occur and a radical anion is formed. For such a species obviously hyperfine splitting arising from the hydroxylic proton can no longer be observed. To be sure, in some cases the corresponding hyperfine splitting is not observed owing to a strong temperature dependence of a(OH), which can assume values close to zero over a limited temperature range. This is the case, for example, of the hydroxyethyl radical as reported by *Livingston & Zeldes* [25].

The interaction of dissolved radicals and solvent is thus basically of two types:

Weak interaction (section 4.3.1): The radical R–OH and the solvent form an associate in the sense of *Lewis*

$$R{-}OH + n\,L \rightleftarrows R{-}OH\cdots L_n \tag{11}$$

Strong interaction (section 4.3.2): The radical R–OH acts as a *Brönsted* acid (or base) and transfer (or accepts) a proton to (from) the solvent.

$$R{-}OH + nL \rightleftarrows R{-}O^- + HL_n^+$$

$$R{-}OH + nL \rightleftarrows R{-}OH_2^+ + L_n^- \tag{12}$$

4.3.1. *Weak interaction.* This case is more effectively visualized by the solvent dependence of the hyperfine splitting pattern of the ESR. spectrum of the 3-hydroxy-2-butenyl-2-oxyl radical (**V**-H). In the solvent systems used *(cf. Table 1 )* the hydroxylic proton is never transferred to the solvent because its hyperfine splitting can always be observed. Some of the splitting constants show a very strong relative change in magnitude with solvent variation (*e.g.* about 25% for a change from a polar to an non-polar sovent, *cf. Table 1*). The relative ordering between the smaller of the methyl couplings and the hydroxylic coupling is inverted when changing from carbon tetrachloride/toluene to methanol/toluene and the couplings are coincidentally identical in methylenechloride/acetonitrile.

In solution, the polar radical very probably forms an associate with the solvent molecules. From ESR. data of the dissolved radical alone it is hardly possible to draw any conclusion about the nature of such a short-lived complex. However, for the case of *p*-semibenzoquinone radical, *Spanget-Larssen* [30] has recently performed an INDO calculation in which the solvent is represented by point charges

and has obtained a good agreement between measured and calculated coupling constants. Besides the fact that this approach requires full geometry optimization and the introduction of a rather arbitrary crystal field of the solvent, reservations apply to the INDO method for prediction of coupling constants in general. As a consequence, for a correlation of the coupling constants in a large number of substituted phenoxy radicals, *Dixon et al.* [21] had to resort to a graphical method. Furthermore, in the case of the 2-hydroxyethenyloxyl radical (**IV**-H), a comparison of the result obtained by INDO and *ab initio* methods indicated very serious discrepancies in the electronic structure obtained by these two methods [18].

4.3.2. *Strong interaction.* This case is exemplified by the solvent dependence of the ESR. spectrum of the 2-hydroxyphenoxyl radical (**I**-H, $\mathbf{I}^-$). The ESR. spectrum of **I**-$H_2$ irradiated in methanol consists of three triplets *(cf. Fig. 1a)*. Similar spectra have been obtained in aqueous solution and assigned to the neutral radical **I**-H [31] [32]. However, the spectrum obtained with addition of base to the methanolic solution is practically the same as without base *(cf. Fig. 1a)*. Thus it is probable that the radical present in a hydroxylic solvent is not the neutral **I**-H but rather the radical anion $\mathbf{I}^-$. In fact, we found that **I**-H is exclusively formed in a neutral aprotic solvent [11] owing to the fact that the intrinsic acidity of the radical **I**-H is much higher (about 3 p$K$ units) than that of the parent compound **I**-$H_2$ [33].

In the solvent system carbon tetrachloride/triethylamine/dioxane it is possible to obtain, in addition to the pure anionic form $\mathbf{I}^-$ (triethylamine $\approx 10^{-1}$ M) and the pure neutral form **I**-H, the superposition of both forms in any desired relative concentration (*cf.* [10]). As a model calculation fully confirmed *(cf. Fig. 1)* the exchange between $\mathbf{I}^-$ and **I**-H is slow in this particular solvent system and it is therefore possible to distinguish between the two radical species. Upper limits for the exchange rates can therefore be determined by simulation and are listed in the key of *Figure 1*.

The case of the protonation equilibrium **I**-H $\leftrightarrows$ **I**-$H_2^+$ leads on the contrary to a fast exchange between the two radicalic forms and has been treated in detail in a previous paper [14].

Deprotonation of the 2-amino-phenoxyl (**III**-$H_2$) could not be achieved at the same base concentration which is effective for 2-hydroxyphenoxyl. This constitutes chemical evidence for the assignment of the proton to the amino rather than to the oxy group, because the former is a much weaker acid than the latter.

Finally in contrast to the 2-hydroxy-butenyl oxy radical (**V**-H) the 1,2-diphenyl-1-hydroxy-ethenyl oxy radical (**VI**-H) is deprotonated in methanolic solution *(cf. Fig. 5)* since the two phenyl groups become equivalent and the spectrum remains essentially unchanged upon the addition of base. This latter spectrum is identical with that reported by *Dehl* [27] and assigned to the anion $\mathbf{VI}^-$. The different observed acidity of radicals **V**-H and **VI**-H makes chemically sense in view of the much larger $\pi$-system available to the negative charge for delocalization in the benzil anion.

The authors express special gratitude to Prof. *Hs. H. Günthard* for support and encouragement of this work. Financial support by the *Eidgenössische Stiftung zur Förderung schweizerischer Volkswirtschaft durch wissenschaftliche Forschung* and a generous stipend by *Sandoz AG*, Basle, are gratefully acknowledged. The computer programs ESREXN and ESREX, used in the analysis of the ESR. spectra. were kindly supplied by Dr. *J. Heinzer.*

## REFERENCES

[1] *E. E. Tucker & E. Lippert*, The Hydrogen Bond, North Holland Publishing Company, Amsterdam 1976. Ed. P. Schuster, G. Zundel & C. Sandorfy.
[2] *S. S. Eaton & G. R. Eaton*, J. Am. Chem. Soc. *99*, 1604 (1977).
[3] *J. Henning & H. H. Limbach*, J. Chem. Soc. Faraday II *75*, 752 (1969).
[4] *F. Graf*, Chem. Phys. Lett. *62*, 291 (1979).
[5] *H. H. Limbach & W. Seiffert*, Ber. Bunsenges. Phys. Chem. *78*, 641 (1974).
[6] *J. R. Bolton, A. Carrington & P. F. Todd*, Mol. Phys. *6*, 169 (1963).
[7] *T. E. Gough*, Can. J. Chem. *47*, 331 (1969).
[8] *H. Fischer*, Mol. Phys. *9*, 169 (1965).
[9] *P. J. Krusic, P. Meakin & J. P. Jesson*, J. Phys. Chem. *75*, 3438 (1971)
[10] *T.-Kyu Ha*, Chem. Phys. Lett. *30*, 379 (1975).
[11] *K. Loth, F. Graf & Hs. H. Günthard*, Chem. Phys. *13*, 95 (1975).
[12] *A. I. Prokofiev, N. N. Bubnov, S. P. Solodovnikov & M. I. Kabachnik*, Tetrahedron Lett. *28*, 163 (1974).
[13] *M. Rudin, K. Loth, F. Graf & Hs. H. Günthard*, Chem. Phys. Lett. *46*, 29 (1977).
[14] *K. Loth, F. Graf & Hs. H. Günthard*, Chem. Phys. Lett. *45*, 191 (1977).
[15] *A. Carrington & A. D. McLachlan*, 'Introduction to Magnetic Resonance', Harper's International Edition 1969, Chapter 12.
[16] *J. Brinckmann & H. Zimmermann*, Z. Naturforsch. A *23*, 1 (1968).
[17] *J. H. Freed & G. K. Fraenkel*, J. Chem. Phys. *38*, 2040 (1963).
[18] *F. Graf, K. Loth, M. Rudin, M. Forster, T. Kyu Ha & Hs. H. Günthard*, Chem. Phys. *23*, 327 (1977).
[19] *F. Graf, K. Loth & Hs. H. Günthard*, Helv. Chim. Acta *60*, 710 (1977).
[20] *P. Neta & R. W. Fessenden*, J. Phys. Chem. *78*, 523 (1974).
[21] *W. T. Dixon, M. Moghimi & D. Murphy*, J. Chem. Soc. Faraday II *70*, 1714 (1974).
[22] *J. A. Pople & D. L. Beveridge*, 'Approximate Molecular Orbital Theory', McGraw-Hill, New York 1970.
*P. A. Dobosh*, CNINDO: CNDO and INDO, Molecular Orbital Program, Quantum Chemistry Program Exchange, Program No. 142, Indiana University.
[23] *D. Lister, J. K. Tyler, J. H. Hog & N. W. Larsen*, Mol. Struct. *23*, 253 (1974).
[24] *C. E. Dykstra & H. F. Schäfer*, J. Am. Chem. Soc. *98*, 401 (1976).
[25] *H. Zeldes & R. Livingston*, J. Chem. Phys. *47*, 1465 (1967).
[26] *M. Forster*, Thesis; Federal Inst. of Technology (ETH), Zürich, No. 6180, 1978.
[27] *R. Dehl & G. K. Fraenkel*, J. Chem. Phys. *39*, 1793 (1963).
[28] *E. W. Stone & A. M. Maki*, J. Chem. Phys. *36*, 1944 (1962).
[29] *P. Ackermann, F. Barbarin, J. P. Germain, C. Fabre & B. Tchoubar*, Tetrahedron *30*, 1019 (1974).
[30] *J. Spanget-Larssen*, Chem. Phys. Lett. *44*, 543 (1976).
[31] *A. Carrington & I. C. P. Smith*, Mol. Phys. *8*, 101 (1964).
[32] *W. T. Dixon & D. Murphy*, J. Chem. Soc. Faraday II *72*, 135 (1975).
[33] *E. Hayon & M. Simic*, Acc. Chem. Res. *7*, 114 (1974).
[34] *J. Heinzer*, Mol. Phys. *22*, 167 (1971).
[35] *J. A. Pople, D. L. Beveridge & P. A. Dobosh*, J. Am. Chem. Soc. *90*, 4201 (1968).
[36] *G. A. Russel, G. Wallraff & J. L. Gerlock*, J. Phys. Chem. *82*, 1161 (1978).